Preparation of Confined, One-Dimensional Boron Nitride Chains in the 1-D Pores of Siliceous Zeolites under High Pressure, High Temperature Conditions

Damian Paliwoda, Marco Fabbiani, Mélanie Wynn, Frederico Alabarse, Anja Rosenthal, Wilson Crichton, Leszek Konczewicz, Michal Bockowski, David Maurin, Thierry Michel, et al.

HAL Id: hal-03884890

https://hal.umontpellier.fr/hal-03884890v1

Submitted on 31 Oct 2023

Preparation of Confined, One-Dimensional Boron Nitride Chains in the 1-D Pores of Siliceous Zeolites under High Pressure, High Temperature Conditions

Damian Paliwoda†, Marco Fabbiani†, Mélanie Wynn‡, Frederico Alabarse‖, Anja Rosenthal▽$,

Wilson Crichton▽, Leszek Konczewicz▲▪, Michal Bockowski▪, David Maurin▲, Thierry Michel▲,

Umit B. Demirci§, Jérôme Rouquette†, Patrick Hermet †, Francesco di Renzo†, Arie van der

Lee§, Guillaume Cassabois▲, Samuel Bernard‡, Julien Haines*†

† ICGM, CNRS, Université de Montpellier, ENSCM, Montpellier, France.

‖Elettra Sincrotrone Trieste, Trieste, Italy

▽ESRF - The European Synchrotron, 71 Avenue des Martyrs, Grenoble, France

$Research School of Earth Sciences, The Australian National University, Canberra, ACT 2601, Australia

▲Laboratoire Charles Coulomb, UMR 5221 CNRS, Université de Montpellier, Montpellier, France.

▪Institute of High-Pressure Physics, Polish Academy of Sciences, Sokolowska 29/37

01-142 Warsaw, Poland

1

§Institut Européen des Membranes, IEM – UMR 5635, Universite de Montpellier, ENSCM,

CNRS, 34090 Montpellier, France.

‡CNRS, IRCER, UMR 7315, University of Limoges, F-87000 Limoges, France

AUTHOR INFORMATION

Corresponding Author

*Julien Haines

  Tel: +33448792114

Julien.Haines@umontpellier.fr

ABSTRACT. Low dimensional boron nitride (BN) chains were prepared in the one-dimensional pores of the siliceous zeolites theta-one (TON) and Mobil-twelve (MTW) by the infiltration, followed by the dehydrocoupling and pyrolysis of ammonia borane under high pressure, high temperature conditions. High-pressure x-ray diffraction in a diamond anvil cell and in a large volume device was used to follow *in situ* these different steps in order to determine the optimal conditions for this process. Based on these results, millimeter-sized samples of BN/TON and BN/MTW were synthesized. Characteristic B-N stretching vibrations of low-dimensional BN were observed by infrared and Raman spectroscopies. The crystal structures were determined using a combination of x-ray diffraction and density functional theory with one and two one-dimensional zig-zag $(BN)_x$ chains per pore in BN/TON and BN/MTW, respectively. These 1-D BN chains potentially have interesting photoluminescence properties in the far ultraviolet region of the electromagnetic spectrum.

Introduction

Due to its large band gap (6 eV), layered hexagonal boron nitride (h-BN) is a material of choice as a light-emitting diode (LED) source in the far ultraviolet (FUV)[1-3]. This indirect gap material[4] exhibits record UV light-emission properties and is thus of great interest for the next generation of FUV LEDs.

Nanostructured 1-dimensional forms of BN[5-6] can be prepared in and on carbon nanotubes (CNT). Single wall BN nanotubes with a diameter of 7 Å can, for example, be prepared from the molecular precursor ammonia borane, NH_3BH_3 (AB), in CNTs at high temperature and retain the high band gap of bulk h-BN. Theoretical studies[7-8] predict a transition to a direct bandgap for BN monolayers (2D) or nanotubes (1D) with a higher radiative yield. This has been confirmed experimentally[9-11] in the case of 2D monolayers of h-BN; however, there are no reports in the literature on the FUV emission properties of the 1-D nanostructures.

The use of the 4-7 Å micropores of selected zeolites allows the preparation of BN nanostructures with even lower dimensions. Previous work has shown that purified ammonia borane (AB) with a Van der Waal's diameter of 3.8 Å, can be readily incorporated at room temperature using moderate pressures[12] in the micropores of the siliceous zeolites MFI, with a three-dimensional pore system with a diameter of 5.5Å, and TON, with a one-dimensional elliptical 5.5x4.7 Å pore system. In the latter case, hydrogen release was investigated upon heating the TON/AB composite under pressure at relatively moderate temperatures below 300°C giving rise to the polymerization and dehydrocoupling of ammonia borane to form polyaminoborane $(NH_2BH_2)_n$ and then polyiminoborane $(BNH_x)_n$ chains confined in the pores of the host TON zeolite[13]. Such confined chains could potentially be converted to 1-D BN chains by pyrolysis at high temperatures.

In the present work, the formation of 1-D BN chains is investigated in TON and a second zeolite MTW with larger 5.7 Å x 6.8 Å diameter pores, Figure 1. The insertion, dehydrocoupling and polymerization of AB in these host zeolites is investigated *in situ* by x-ray diffraction. Millimeter-sized samples are prepared in a large volume high-pressure device and the BN chains are characterized by spectroscopic and diffraction techniques coupled with density functional theory calculations.
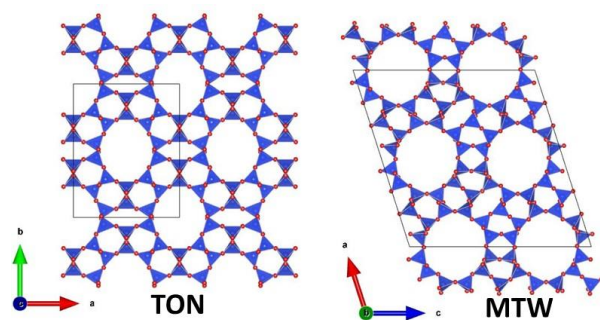

Figure 1. Crystal structures of TON and MTW.

Experimental and Theoretical Methods

Polycrystalline MTW, synthesized as described previously[14], and purified ammonia borane (AB) were loaded in a resistively-heated diamond anvil cell under an inert atmosphere in a glove box. Ruby was used as a pressure calibrant. The pressure was estimated from the shift in the R_1 fluorescence line of ruby corrected for the sample temperature[15-16]. The temperature was measured with a thermocouple placed on the diamond anvil. High pressure synchrotron X-ray diffraction (λ=0.4957 A) measurements in the diamond anvil cell were performed with an 80 μm beam spot on the sample up to 2 GPa and up to 280°C on the Xpress beamline equipped with a PILATUS3 S 6M (DECTRIS) detector at the ELETTRA Sincrotrone Trieste (Trieste, Italy). The sample-to-detector distance was 634.38 mm. Recovered samples were studied using the same set up, but with

a sample-to-detector distance of 950.69 mm. The XRD images were converted to 1-D diffraction profiles using Dioptas[17]. Rietveld refinements were performed using Fullprof[18] and crystal structures plotted using Vesta[19]. Soft constraints were applied to the Si-O and O-O distances. An overall isotropic atomic displacement parameter (ADP) was used for all atoms as no improvement was obtained using individual ADPs. As in previous work[20-21], residual electron density, which may arise from residue of the structure directing agent, was modelled using carbon or nitrogen atoms with partial occupancy placed on the maxima of electron density.

X-ray diffraction measurements (λ=0.389153 Å) under pressure in a multi-anvil press using a monochromatic incident beam were performed on the ID06-LVP beamline at the European Synchrotron Radiation Facility (Grenoble, France) equipped with a Dectris Pilatus900k-W detector at 1999.385 mm from the sample. The powdered TON (synthesized as described previously[14]) or MTW samples along with AB were loaded in NaCl capsules (2.2 mm inner diameter, 2.9 mm height) in a glove box, which were placed in a graphite heater in a 14/8 octahedral assembly. Temperature was monitored using a D-type thermocouple. Pressure estimates were by diffraction combined with the equation of state of NaCl[22]. Experiments were conducted at pressures up to 3 GPa and temperatures up to 500°C.

Large-volume synthesis experiments were performed in a typical experimental setup for gallium nitride (GaN) crystal growth with the high nitrogen pressure solution (HNPS) method[23]. A vertically positioned, technological gas pressure reactor with an internal diameter of 4 cm was used. A multizone cylindrical graphite furnace was placed inside the gas pressure chamber. The MTW-AB or TON-AB mixtures (200 mg of zeolite and 50 mg of AB) were loaded in sealed metallic capsules in a glove box and then placed in the graphite crucible in the furnace of the high pressure reactor. To monitor the temperature during the experiments, PtRh6%–PtRh30%

thermocouples were used. They were arranged along the furnace and coupled with the input power control electronic systems. The pressure was measured by manganin gauges positioned in the low temperature zone of the reactor. The pressure and temperature were stabilized with an accuracy of 1 MPa and 0.1 K, respectively. Helium gas was used as a pressure transmitting medium. The samples were pressurized to 0.8 GPa and then heated to 800°C followed by cooling to room temperature and decompression.

Raman spectra were obtained on a Renishaw inVia Raman Microscope using a 633nm He-Ne laser for excitation (9mW at the sample). The scattered light was collected through x5 objective (NA = 0.12) using a backscattering configuration. Additional measurements on a Horiba Xplora Raman microspectrometer were carried out using a 532 Nm Nd-YAG laser. Infrared spectroscopic measurements on the large-volume samples were performed on a Bruker Tensor 27 FT-IR spectrometer using an attenuated total reflectance (ATR) accessory.

Calculations were carried out within the density functional theory framework as implemented in the SIESTA package[24]. We used the generalized gradient approximation (GGA) to the exchange correlation functional as proposed by Perdew, Burke and Ernzerhof (PBE)[25]. Core electrons are replaced by nonlocal norm-conserving pseudopotentials. The valence electrons are described by a double-zeta singly polarized basis set. The localization of the basis is controlled by an energy shift of 50 meV. Real space integration is performed on a regular grid corresponding to a plane-wave cutoff of 350 Ry. Van der Waals corrections (DFT-D3) are included in our calculations using the semi-empirical dispersion potential parametrized by Grimme[26].

The structures were considered as relaxed when the maximum residual atomic force was smaller than 0.02 eV/Å and the pressure below 2×10^{-5} eV/Å^3. The k-points mesh for MTW-BN and TON-

BN was fixed to 5x7x5 and 6x6x10, respectively. For the calculation of the density-of-states, these meshes were much denser and fixed to 14x14x10 for MTW-BN and to 14x14x20 for TON-BN. The electron localization function (ELF)[27] was calculated for MTW-BN using the ABINIT package[28].

Results

In situ high P, high T investigation of the MTW-AB system in a diamond anvil cell

Upon closing the DAC at 0.05 GPa, the sample consisted of two phases, tetragonal ammonia borane and the MTW zeolite, Figure 2. The structure of the MTW zeolite was refined using the Rietveld method (CCDC 2191261). As compared to empty MTW, decreased intensities for the low angle reflections were observed from 0.05 GPa, Figure 2, providing a strong indication that some AB molecules had entered the pores of MTW as observed previously for the zeolites MFI[12] and TON[13]. Fourier difference maps allowed the identification of the possible sites for the AB molecules in the pores. The resulting model with isoelectronic argon atoms representing disordered AB molecules was used as a starting point for Rietveld refinements (Figure 3). In contrast to TON[13], the Fourier difference maps only permitted to locate the center of gravity of the molecules. This could indicate either that the molecules are more mobile in the larger pores of MTW or that less information is available on the maps due to the lower symmetry and larger unit cell of MTW. The refined occupations for the AB sites at 0.05 GPa gave a pore content of 3.5 AB molecules per unit cell (uc). The occupancy increased with further compression at room temperature up to 4.4 AB/uc at 1.0 GPa (Figure S1 in SM, CCDC 2207771). This occupancy is intermediate between those of TON[13] and MFI[12], when normalized to 24 SiO_2 units: 1.2 (TON), 1.9 (MTW) and 2.6

(MFI). These values scale with the accessible pore volumes of the three materials, which are linked to pore diameter and dimensionality (1D or 3D): 0.10 cm^3/g (TON)[29], 0.14 cm^3/g (MTW)[21] and 0.196 cm^3/g (MFI)[30]. These results indicate that the pores of these three zeolites fill in a similar manner with AB molecules and support the accuracy of the filling assessment based on refined occupancies.

The sample was then slowly heated, which resulted in a continuous increase in pressure. The bulk AB was found to begin to transform to the orthorhombic $Cmc2_1$ high pressure phase[31] at 1.0 GPa and 50°C. The AB content remained essentially constant up to 106°C and 1.7 GPa (Figure S2, CCDC 2207772). This is also consistent with the observed relative volumes of the MTW-AB system, which are much greater than those of empty MTW, but at the same time decrease gradually on compression in a similar way to a compound with a fixed chemical composition, Figure 4.
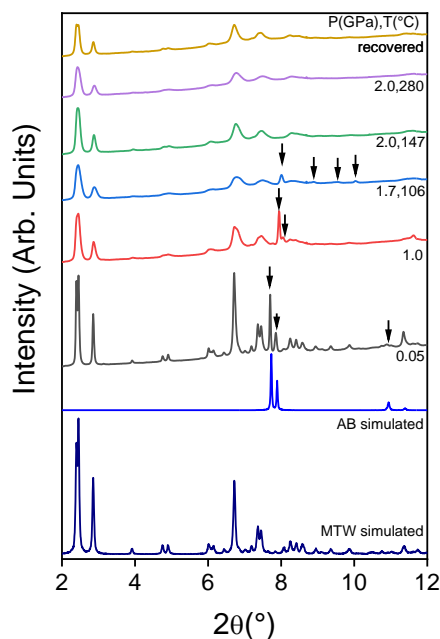
Figure 2. X-ray diffraction patterns (λ=0.4957 Å) of the MTW – (B-N-H) system as a function of pressure and temperature. Simulated XRD patterns for AB and for empty MTW are given for comparison. Arrows indicate the principal AB reflections.

The following points were obtained above the dehydrocoupling and polymerization temperatures of AB[31] around 125°C at 2.0 GPa leading to the formation of polyaminoborane $(NH_2BH_2)_n$. A volume *increase* of 0.9 % was observed for the first point at 147°C and 2 GPa (Figure S3, CCDC 2207773). Volume increases at high pressure and high temperature were previously observed for TON[13] and were linked to the formation and insertion of H_2 in the pores. Further H_2 loss from polyaminoborane $(NH_2BH_2)_n$ occurs at around 180°C and 2 GPa with the formation of polyiminoborane $(BNH_x)_n$. A further volume increase occurs at the next point at 197°C and 1.9 GPa (Figure S4, CCDC 2207774). The volume then decreases slightly at the highest temperature reached and then decreases continuously on cooling and decompression finally reaching similar

values to empty MTW[21]. A strong volume decrease on cooling was also observed for TON[13] and was linked to changes in the quantity and volume occupied by H_2 in the pores. Over the P-T cycle, the pore content in equivalent AB molecules remained typically close to 4 (see deposited CCDC files).
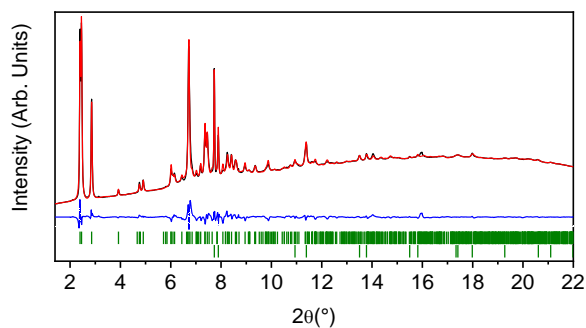

Figure 3. Experimental (black), calculated (red) and difference (blue) profiles (λ=0.4957 Å) for Rietveld refinement of the *C*2/*c* structure of MTW-NH₃BH₃ at 0.05 GPa and 23°C. Vertical bars indicate the calculated positions of the Bragg reflections. The lower row of markers corresponds to the tetragonal phase of BH₃NH₃, space group *I*4*mm*.
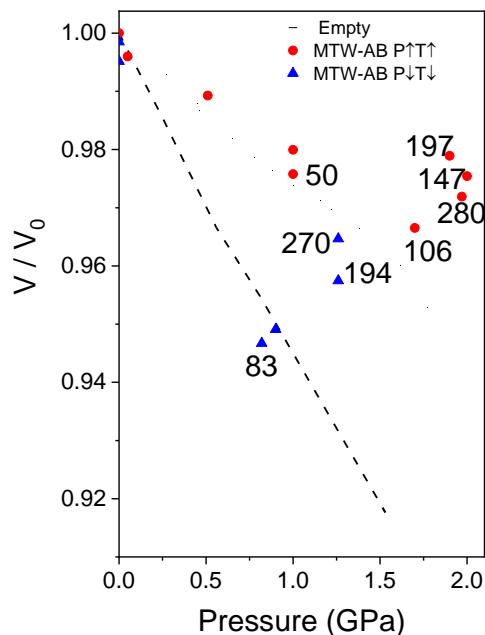
Figure 4. Relative volume of the MTW – (B-N-H) system as a function of pressure. Temperatures are given in °C. Data for empty MTW[21] are given for comparison.

In situ high P, high T investigation of the MTW-AB and TON-AB systems in a large volume, multianvil press

The MTW-AB and the TON-AB were studied in situ by x-ray diffraction at pressures up to 3 GPa and temperatures up to 500°C in a multianvil device, Figure 5, to determine the stability of the zeolite-based composite materials under these conditions. The phase transition from the high pressure $Cmc2_1$ phase to the high pressure, high temperature $Pnma$ form of AB[32] was observed at close to 3 GPa and 120°C based on the appearance of new reflections between 5.5° ($d = 4.06$ Å) and 7° ($d = 3.19$ Å) in 2θ. Upon further heating the diffraction lines of AB disappear, in particular

12

the strong reflection near 6.4° ($d = 3.49$ Å), and the peaks of the host zeolites shift to lower angles as observed previously for both systems in diamond anvil cells. The loss of the AB peaks correspond to the formation of amorphous polyaminoborane $(NH_2BH_2)_n$ and the shift in the diffraction peaks to lower angles was found to be due to the insertion of hydrogen in the structures of the zeolites as discussed in the previous section. No major changes, except for broadening of the diffraction lines, were observed up to the highest temperatures (500°C), confirming the stability of the filled zeolites under these conditions with respect to dense silica forms such as quartz and coesite. Transitions have been observed in other zeolites at similar pressures (2.5 GPa) and higher temperatures (800°C)[33]. Raman measurements (Figure S5) on the recovered samples indicated the presence of turbostratic BN with very broad peaks near 1373 cm^{-1} with FWHM values of 39 cm^{-1} for TON-BNH$_x$ and 56 cm^{-1} for MTW-BNH$_x$. These measurements also showed that the conversion to BN was incomplete as medium intensity N-H stretching peaks are observed around 3430 cm^{-1}, indicating that a significant amount of polyiminoborane $(BNH_x)_n$ remains. These results suggest the application of higher temperatures to reduce the amount of polyiminoborane and lower

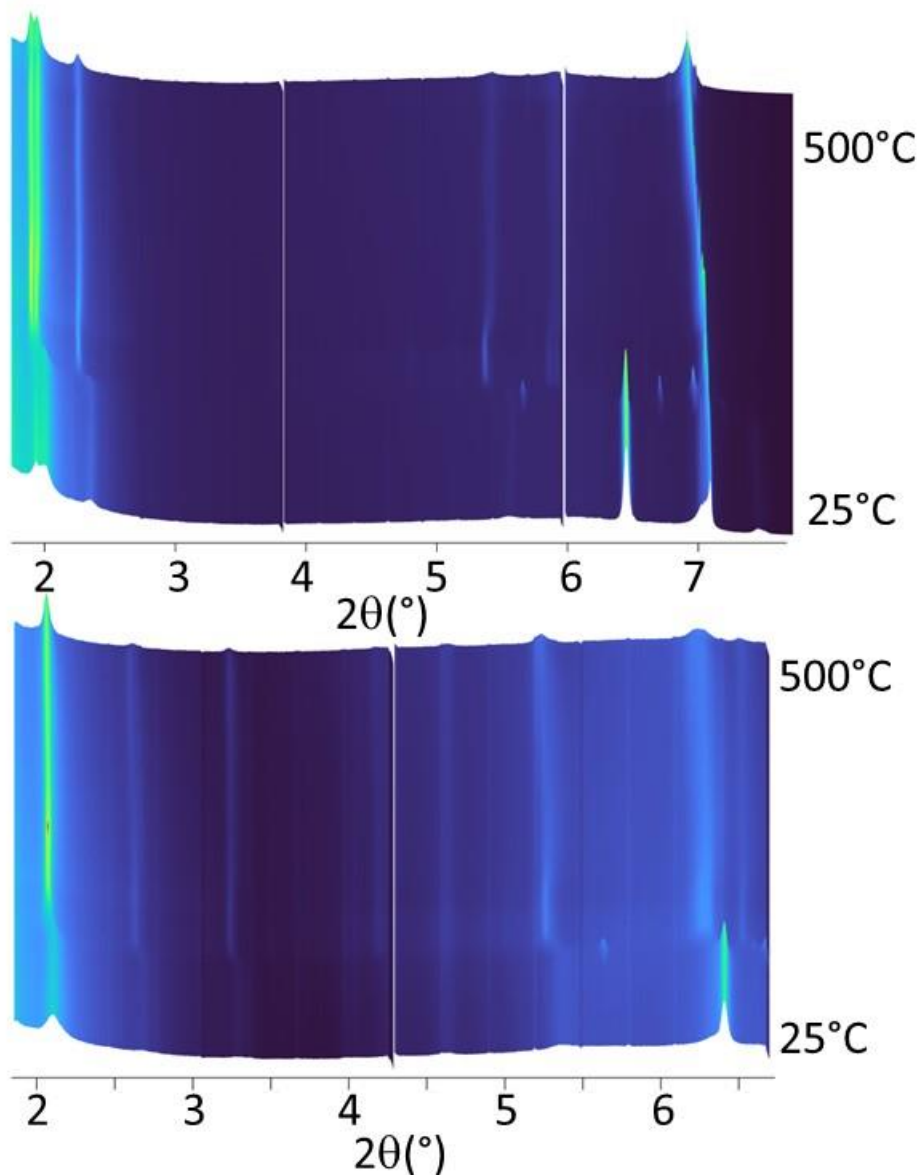pressures to avoid transitions in the zeolites in order to achieve optimal conditions for the process.

Figure 5. 2D heat plots of the diffraction data (λ=0.389153 Å) for the MTW/B-N-H at 3.0(1) GPa (above) and the TON/B-N-H at 2.8(1) GPa (below) systems as a function of T. The strong lines just above 7° (d = 3.19 Å) in the upper plot are from the NaCl pressure calibrant and from the graphite furnace.

Characterization of MTW-BN and TON-BN synthesized in a large volume, gas pressure reactor

The MTW-AB and the TON-AB were treated at 0.8 GPa and 800°C for one hour in the large volume, gas pressure reactor. The recovered samples were analyzed by Raman and infrared spectroscopy and x-ray diffraction. In the Raman spectra of the recovered samples (Figure 6), a strong peak was observed at 1379 cm^{-1} and 1375 cm^{-1} respectively, indicating the formation of boron nitride. These peaks are shifted to higher wavenumber and are broadened with respect to bulk BN[34], for which the peak is observed at 1366 cm^{-1}. The FWHM were 29 cm^{-1} and 42 cm^{-1}, respectively as compared to 8 cm^{-1} for well crystallized hBN[34]. Poorly crystallized, turbostratic BN obtained from treating AB under N_2 at 1800°C[35] exhibited a peak at 1369.1 cm^{-1}, which is intermediate between the confined BN in the zeolites and bulk crystalline BN. Very weak peaks in the N-H stretching region were observed indicating trace amounts of hydrogen containing polymers, such as polyiminoborane $(BNH_x)_n$, remain as found previously for BN synthesized from AB even after heating above 1400°C. At lower wavenumbers, the sharp Si-O stretching and bending modes of the crystalline host zeolites were observed, Table 1, confirming the stability of the filled zeolites under these conditions. The bending modes in particular, between 300-500 cm^{-1}, are well defined due to the characteristic rings of corner sharing SiO_4 tetrahedra in TON (5, 6 and 10 membered rings - MR) and MTW (4, 5, 6 and 12 MR). In the infrared spectra (Figure 7), the corresponding modes are observed at 1376 cm^{-1} and 1370 cm^{-1} respectively. These values are higher than that of hBN single crystals[36] for which the mode is observed at 1365 cm^{-1} and also of that of turbostratic BN[37] for which the peak is observed at 1344 cm^{-1}. It can be noted that such shifts have been observed for thin films consisting of few BN layers, for which the mode decrease from 1379 cm^{-1} to 1368 cm^{-1} when going from 1 to 10 layers[36]. Again, at lower wavenumbers strong modes corresponding to the Si-O stretching and bending of the host zeolites are observed.

The positions of these peaks are very similar, apart from the reduction in wavenumber of up to 3 cm^{-1} for certain modes in the 500-700 cm^{-1} range, to those observed for unfilled TON and MTW (Figure 7). There are also some differences in the linewidth. The present results show that the vibrational signature of the BN confined in the pores is distinct from that of turbostratic BN, which was found from x-ray diffraction (see below) to be present as a secondary phase due to the transformation of excess AB outside the pores of the zeolites to BN. The contribution from turbostratic BN can be seen particularly in the IR data as shoulders near 1344 cm^{-1}, 26-32 cm^{-1} lower than the frequencies of the stretching modes of confined BN. Any contribution in the Raman spectra cannot be distinguished clearly, but will give rise to some additional broadening on the low wavenumber side on the stretching peak of the confined BN.
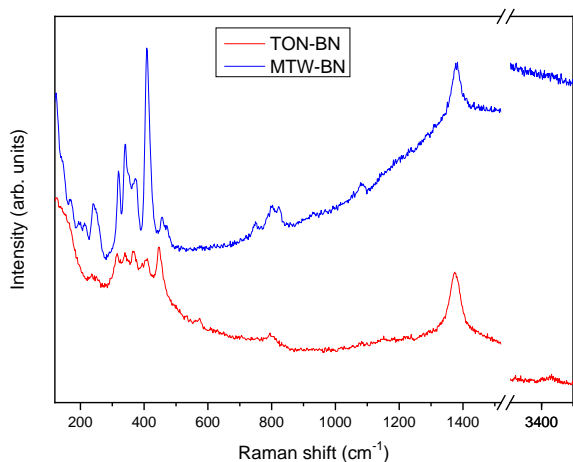

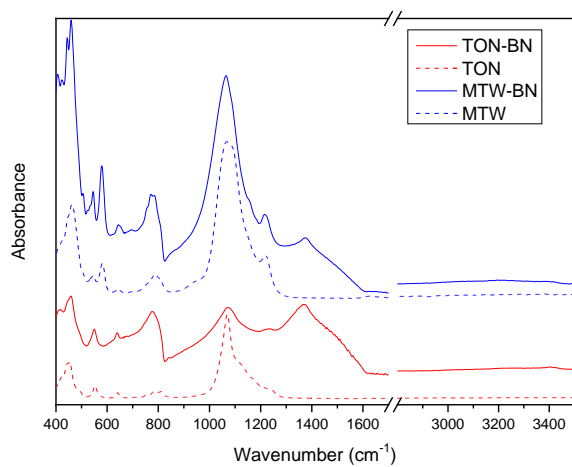**Figure 6. Raman spectra of recovered TON/BN and MTW/BN composites**.

16

Figure 7. ATR IR spectra of recovered TON/BN and MTW/BN composites and calcined, empty TON and MTW.

Table I: Raman and IR peak assignments for the MTW-BN and TON-BN nanocomposites. Apart from the B-N stretching and bending, all modes are due to the SiO_2 framework. (s=strong, m=medium, w=weak, sh=shoulder, br=broad, v=very)

MTW-BN		TON-BN		
Raman shift (cm^{-1})	IR Wavenumber (cm^{-1})	Raman shift (cm^{-1})	IR Wavenumber (cm^{-1})	Assignment
3431vvw	3400vvw	3429vw	3407vw	N-H stretch
	3207vvw		3270vw,br	N-H stretch
	3036vvw		3067vw,br	N-H stretch
1379s	1376m	1375s	1370s	B-N stretch
	1220m		1241m	External asym. stretch
			1211sh	
	1158sh		1172sh	
	1089sh		1125sh	
1084w	1064s		1072s	Internal asym. stretch
823m				External sym. stretch
804m	808sh	800w	810sh	External sym. stretch
	786m		783s	
	771m		778s	BN bending
750w	754m		750sh	
	653w			Internal asym. stretch
	643w		638m	Internal asym. stretch
	579m	574w		Secondary building unit ring vibration
	545w		550m	Secondary building unit ring vibration
	532vw			
	506w		489sh	
472m				Si-O bending
457m	459s		458s	Si-O bending
	443s	447s	445sh	
	423m		419m	
411s		407s		
371s		368s		
342s		342s		
321s		316s		
247m		244w		
214w				
197w				
169w				

The MTW-BN and TON-BN samples were studied by x-ray powder diffraction on the Xpress Beamline at the Elettra synchrotron. Both samples were characterized by sharp diffraction lines due to the host zeolite and three broad features around 8.1° (d = 3.51 Å), 13.5° (d = 2.11 Å) and 23.3° (d = 1.23Å), which are linked to poorly crystallized, bulk turbostratic BN[38]. In the Rietveld refinements of the BN-filled zeolites described below, these broad features were included in the background. In both cases, the structures of the empty frameworks were used as starting points and the guest atoms were located using Fourier difference maps. The positions on the Fourier maps corresponded to atomic chains. These were tested as starting points in Rietveld refinements with soft constraints on the B-N distances; however, the distances obtained were typically too long, in the order of 1.6 Å with large standard deviations. Taking into account the low scattering factors of B and N, and in order to have a more physically meaningful structure, the positions on the Fourier maps were used to build starting models to obtain reasonable B-N distances by structural relaxation calculations with DFT, Figure 8. In the calculations, a sp^2 hybridization was considered for BN and no constraint was imposed (all atoms were relaxed). A linear sp hybridization was not considered, as it is not compatible with the crystal symmetry in the case of the zeolite TON. The confined BN chains in TON and MTW obtained in the calculations systematically exhibited a B-N bond length of 1.316 Å and a B-N-B angle of 137-139° at the GGA/PBE level, which is very close to the calculated distance (1.30-1.31 Å) for freestanding linear BN chains in previous DFT calculations[39-41]

The N-B-N angle remained close to 180°. Interestingly, the relaxed structure of an isolated free chain was also calculated; the bond length is identical, but the B-N-B and N-B-N angles are 180° giving a linear chain. The bent chains in the confined structure reduce repulsive interactions between the lone pairs of nitrogen in the BN chains and the oxygen atoms of the framework as evidenced by the electron localization function calculations, Figure 9.

The results were then used for Rietveld refinements, Figure 10, of the BN filled zeolites with the BN atoms fixed to the positions obtained by DFT. Structural data from the DFT calculations are provided as CIF files in supporting information.

In the case of BN-filled MTW prepared in the gas pressure reactor (CCDC 2191262), the unit cell volume increases by 0.7% with respect to empty MTW with the following refined unit cell parameters: a=24.985(2)Å, b=5.0344(3)Å, c=24.385(2)Å and β=107.828(8)°. Fifty percent of this volume expansion occurs along the pore axis. Higher flexibility along the direction of the pore axis is similar to what has been observed in certain other 1-D pores systems and arises principally from changes to T-O-T bridging angles[42]. In the final refined structure, there are 2 BN chains per pore with a fractional occupation of 0.25(1) corresponding to 4 BN/uc.
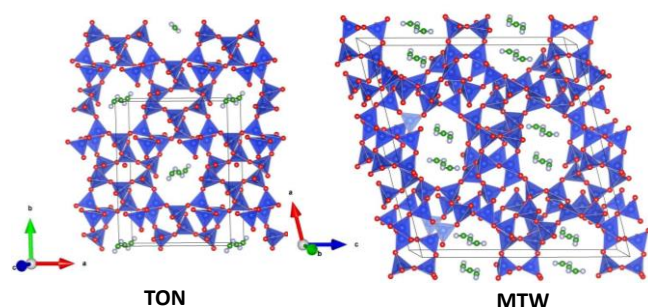

TON   MTW

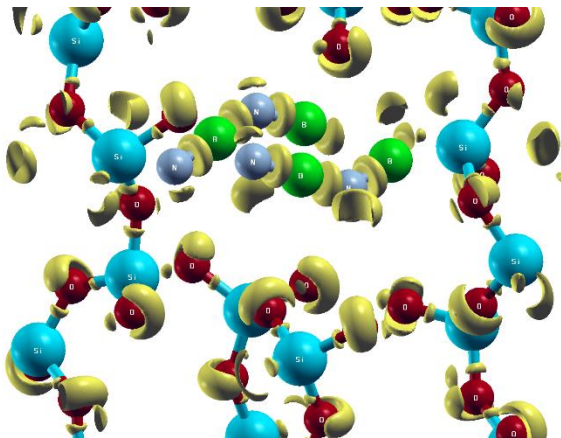**Figure 8. Relaxed crystal structures of TON-BN and MTW-BN.**

Figure 9. Electron localization function (ELF) for an isosurface of 0.85 in MTW-BN. (Note that an ELF value of 1 corresponds to perfect localization[27]).
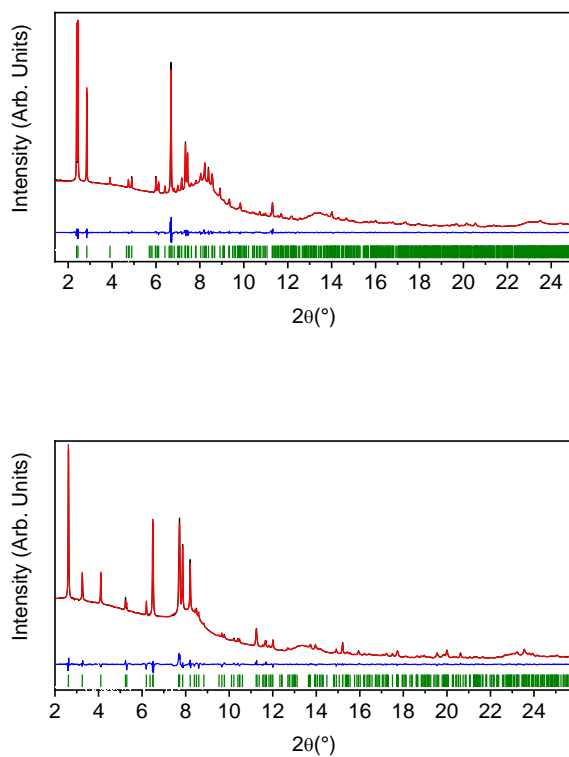

Figure 10. Experimental (black), calculated (red) and difference (blue) profiles (λ=0.4957 Å) for Rietveld refinement of the *C*2/*c* structure of MTW-BN (above) and of the *Cmc*2₁ structure of TON-BN (below). Vertical bars indicate the calculated positions of the Bragg reflections.

In the case of BN-filled TON prepared in the gas pressure reactor (CCDC 2191263), a similar increase in unit cell volume of 0.8% is observed. The refined unit cell parameters are a=13.843(1)Å, b=17.448(2)Å, c=5.0598(5)Å. The expansion is 55% along the pore direction c and the remaining contribution is along b. There is one BN chain per pore with an occupation of 0.54(3) yielding close to 2 BN/uc. In comparing the two zeolites, the cell parameters along the chain directions are similar and the principal differences are the pore diameters of 5.5x4.7 Å pores for TON and 5.7 Å x 6.8 Å pores for MTW providing the necessary space for two bent chains per pore in the latter.

In the case of the bent BN chains in the MTW and TON zeolite hosts, DFT was also used to calculate the electronic density of states (eDOS), Figure 11. The calculated band gap at the GGA/PBE level of these materials are close to 3 eV. It can be seen from the individual contributions to the eDOS from the BN chains and the MTW and TON frameworks that these pure silica zeolites with large band gaps are well suited to host the narrower band gap BN guest chains. The predicted DFT band gap values at the GGA level are well known to be underestimated by about 30-40 % in non-electron-correlated materials. This problem is related to the derivative discontinuity of the exchange-correlation energy[43]. Considering this standard error, the expected, experimental band gap of both materials could be estimated to be around 5 eV, which would yield interesting photoluminescence properties in the UV region of the electromagnetic spectrum. This indicates that composites with 1-D BN chains present distinct properties with respect to more extended structures such as BN nanotubes confined in carbon nanotubes[5-6], which exhibit a similar band gap to hBN.
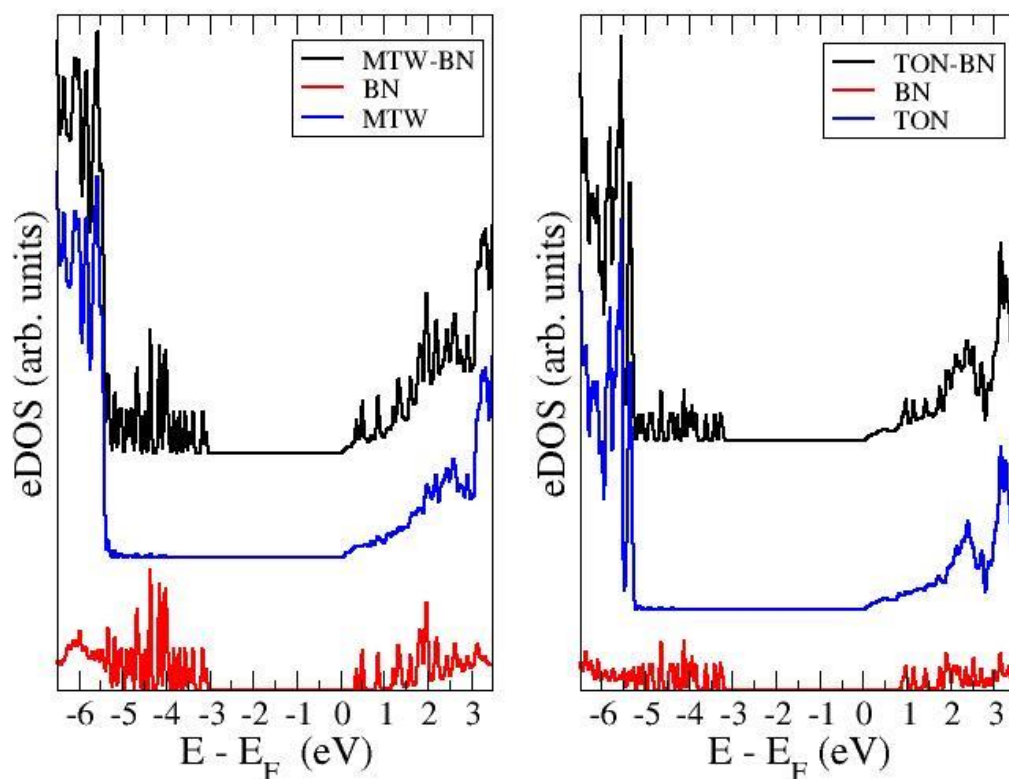
Figure 11. Calculated electronic density of states for MTW-BN (left) and TON-BN (right) with the individual contributions from the host zeolite and the BN chains. E$_F$=Fermi energy.

Conclusions

One-dimensional BN chains were obtained in the pores of the TON and MTW zeolites by insertion followed by polymerization and dehydrocoupling of ammonia borane at high pressure and high temperature. One chain is formed in the 5.5x4.7 Å pores of TON and two chains are formed in the

5.7 Å x 6.8 Å pores of MTW. These chains are bent due to interactions with the framework, thus modifying their electronic structure as compared to isolated linear chains of BN or bulk hBN. These new nanostructures of BN are predicted to exhibit novel UV photoluminescence properties.

ASSOCIATED CONTENT

Supporting Information.

Supplementary figures with the results of Rietveld refinements (S1-S4) and Raman spectroscopy (S5), and Crystallographic information files (CIF) containing the relaxed DFT structural data for MTW-BN and TON-BN have been supplied as supporting information. The following files are available free of charge.

Paliwoda_IC-2022-02430q_SM.pdf (PDF)
MTW_BN_relaxed_DFT.cif (PDF)
TON_BN_relaxed_DFT.cif (PDF)

Accession Codes

CCDC 2191261, 2191262, 2191263, 2207771, 2207772, 2207773, and 2207774 contain the supplementary crystallographic data for this paper. These data can be obtained free of charge via www.ccdc.cam.ac.uk/data_request/cif, or by emailing data_request@ccdc.cam.ac.uk, or by contacting The Cambridge Crystallographic Data Centre, 12 Union Road, Cambridge CB2 1EZ, UK; fax: +44 1223 336033.

AUTHOR INFORMATION

Notes

The manuscript was written through contributions of all authors. All authors have given approval to the final version of the manuscript. The authors declare no competing financial interests.

REFERENCES

1.   Watanabe, K.; Taniguchi, T.; Kanda, H., Direct-Bandgap Properties and Evidence for Ultraviolet Lasing of Hexagonal Boron Nitride Single Crystal. *Nat. Mater.* **2004**, *3*, 404-409.
2.   Kubota, Y.; Watanabe, K.; Tsuda, O.; Taniguchi, T., Deep Ultraviolet Light-Emitting Hexagonal Boron Nitride Synthesized at Atmospheric Pressure. *Science* **2007**, *317*, 932-934.
3.   Watanabe, K.; Taniguchi, T.; Niiyama, T.; Miya, K.; Taniguchi, M., Far-Ultraviolet Plane-Emission Handheld Device Based on Hexagonal Boron Nitride. *Nat. Photonics* **2009**, *3*, 591-594.
4.   Cassabois, G.; Valvin, P.; Gil, B., Hexagonal Boron Nitride Is an Indirect Bandgap Semiconductor. *Nat. Photonics* **2016**, *10*, 262-266.
5.   Nakanishi, R.; Kitaura, R.; Warner, J. H.; Yamamoto, Y.; Arai, S.; Miyata, Y.; Shinohara, H., Thin Single-Wall Bn-Nanotubes Formed inside Carbon Nanotubes. *Scientific Reports* **2013**, *3*, 1385.
6.   Xiang, R.; Inoue, T.; Zheng, Y. J.; Kumamoto, A.; Qian, Y.; Sato, Y.; Liu, M.; Tang, D. M.; Gokhale, D.; Guo, J.; Hisama, K.; Yotsumoto, S.; Ogamoto, T.; Arai, H.; Kobayashi, Y.; Zhang, H.; Hou, B.; Anisimov, A.; Maruyama, M.; Miyata, Y.; Okada, S.; Chiashi, S.; Li, Y.; Kong, J.; Kauppinen, E. I.; Ikuhara, Y.; Suenaga, K.; Maruyama, S., One-Dimensional Van Der Waals Heterostructures. *Science* **2020**, *367*, 537-542.
7.   Blase, X.; Rubio, A.; Louie, S. G.; Cohen, M. L., Quasi-Particle Band-Structure of Bulk Hexagonal Boron-Nitride and Related Systems. *Phys. Rev. B* **1995**, *51*, 6868-6875.

8.   Paleari, F.; Galvani, T.; Amara, H.; Ducastelle, F.; Molina-Sanchez, A.; Wirtz, L., Excitons in Few-Layer Hexagonal Boron Nitride: Davydov Splitting and Surface Localization. *2D Mater.* **2018**, *5*, 045017.

9.   Elias, C.; Valvin, P.; Pelini, T.; Summerfield, A.; Mellor, C. J.; Cheng, T. S.; Eaves, L.; Foxon, C. T.; Beton, P. H.; Novikov, S. V.; Gil, B.; Cassabois, G., Direct Band-Gap Crossover in Epitaxial Monolayer Boron Nitride. *Nat. Commun.* **2019**, *10*, 2639.

10.   Rousseau, A.; Ren, L.; Durand, A.; Valvin, P.; Gil, B.; Watanabe, K.; Taniguchi, T.; Urbaszek, B.; Marie, X.; Robert, C.; Cassabois, G., Monolayer Boron Nitride: Hyperspectral Imaging in the Deep Ultraviolet. *Nano Lett.* **2021**, *21*, 10133-10138.

11.   Cassabois, G.; Fugallo, G.; Elias, C.; Valvin, P.; Rousseau, A.; Gil, B.; Summerfield, A.; Mellor, C. J.; Cheng, T. S.; Eaves, L.; Foxon, C. T.; Beton, P. H.; Lazzeri, M.; Segura, A.; Novikov, S. V., Exciton and Phonon Radiative Linewidths in Monolayer Boron Nitride. *Phys. Rev. X* **2022**, *12*, 011057.

12.   Richard, J.; Cid, S. L.; Rouquette, J.; van der Lee, A.; Bernard, S.; Haines, J., Pressure-Induced Insertion of Ammonia Borane in the Siliceous Zeolite, Silicalite-1F. *J. Phys. Chem. C* **2016**, *120*, 9334-9340.

13.   Paliwoda, D.; Comboni, D.; Poreba, T.; Hanfland, M.; Alabarse, F.; Maurin, D.; Michel, T.; Demirci, U. B.; Rouquette, J.; di Renzo, F.; van der Lee, A.; Bernard, S.; Haines, J., Anomalous Volume Changes in the Siliceous Zeolite Theta-1 TON Due to Hydrogen Insertion under High-Pressure, High-Temperature Conditions. *J. Phys. Chem. Lett.* **2021**, *12*, 5059-5063.

14.   Di Renzo, F.; Remoué, F.; Massiani, P.; Fajula, F.; Figueras, F.; Thierry Des, C., Crystallization Kinetics of Zeolite TON. *Zeolites* **1991**, *11*, 539-548.

15.   Datchi, F.; Dewaele, A.; Loubeyre, P.; Letoullec, R.; Le Godec, Y.; Canny, B., Optical Pressure Sensors for High-Pressure-High-Temperature Studies in a Diamond Anvil Cell. *High Pressure Res.* **2007**, *27*, 447-463.

16.   Shen, G.; Wang, Y.; Dewaele, A.; Wu, C.; Fratanduono, D. E.; Eggert, J.; Klotz, S.; Dziubek, K. F.; Loubeyre, P.; Fat'yanov, O. V.; Asimow, P. D.; Mashimo, T.; Wentzcovitch, R. M. M.; Bass, J.; Bi, Y.; He, D.; Khishchenko, K. V.; Leinenweber, K.; Li, B.; Sakai, T.; Tsuchiya, T.; Shimizu, K.; Yamazaki, D.; Mezouar, M.; Grp, I. T., Toward an International Practical Pressure Scale: A Proposal for an IPPS Ruby Gauge (IPPS-Ruby2020). *High Pressure Res.* **2020**, *40*, 299-314.

17.   Prescher, C.; Prakapenka, V. B., Dioptas: A Program for Reduction of Two-Dimensional X-Ray Diffraction Data and Data Exploration. *High Pressure Res.* **2015**, *35*, 223-230.

18.   Rodriguez-Carvajal, J., Magnetic Structure Determination from Powder Diffraction Using the Program Fullprof. *Applied Crystallography* **2001**, 30-36.

19.   Momma, K.; Izumi, F., VESTA 3 for Three-Dimensional Visualization of Crystal, Volumetric and Morphology Data. *J. Appl. Crystallogr.* **2011**, *44*, 1272-1276.

20.   Thibaud, J. M.; Rouquette, J.; Hermet, P.; Dziubek, K.; Gorelli, F. A.; Santoro, M.; Garbarino, G.; Alabarse, F. G.; Cambon, O.; Di Renzo, F.; van der Lee, A.; Haines, J., High-Pressure Phase Transition, Pore Collapse, and Amorphization in the Siliceous 1D Zeolite, TON. *J. Phys. Chem. C* **2017**, *121*, 4283-4292.

21.   Paliwoda, D.; Fabbiani, M.; Alabarse, F.; Hermet, P.; Rouquette, J.; Di Renzo, F.; Haines, J., Compressibility, Phase Transition, and Argon Insertion in the Siliceous Zeolite Mobil-Twelve at High Pressure. *J. Phys. Chem. C* **2022**, *126*, 2877-2884.

22.   Birch, F., Equation of State and Thermodynamic Parameters of NaCl to 300-kbar in the High-Temperature Domain. *J. Geophys. Res.-Solid* **1986**, *91*, 4949-4954.

23.   Bockowski, M.; Strak, P.; Grzegory, I.; Porowski, S., High Pressure Solution Growth of Gallium Nitride. *Springer Ser. Mater. S* **2010**, *133*, 207-234.

24.   SanchezPortal, D.; Ordejon, P.; Artacho, E.; Soler, J. M., Density-Functional Method for Very Large Systems with LCAO Basis Sets. *Int. J. Quantum Chem.* **1997**, *65*, 453-461.

25.   Perdew, J. P.; Burke, K.; Ernzerhof, M., Generalized Gradient Approximation Made Simple. *Phys. Rev. Lett.* **1996**, *77*, 3865-3868.

26.   Grimme, S., Semiempirical GGA-Type Density Functional Constructed with a Long-Range Dispersion Correction. *J. Comput. Chem.* **2006**, *27*, 1787-1799.

27.   Becke, A. D.; Edgecombe, K. E., A Simple Measure of Electron Localization in Atomic and Molecular-Systems. *J. Chem. Phys.* **1990**, *92*, 5397-5403.

28.   Gonze, X.; Amadon, B.; Anglade, P. M.; Beuken, J. M.; Bottin, F.; Boulanger, P.; Bruneval, F.; Caliste, D.; Caracas, R.; Cote, M.; Deutsch, T.; Genovese, L.; Ghosez, P.; Giantomassi, M.; Goedecker, S.; Hamann, D. R.; Hermet, P.; Jollet, F.; Jomard, G.; Leroux, S.; Mancini, M.; Mazevet, S.; Oliveira, M. J. T.; Onida, G.; Pouillon, Y.; Rangel, T.; Rignanese, G. M.; Sangalli, D.; Shaltaf, R.; Torrent, M.; Verstraete, M. J.; Zerah, G.; Zwanziger, J. W. ABINIT: First-Principles Approach to Material and Nanosystem Properties. *Comput. Phys. Commun.* **2009**, *180*, 2582-2615.

29.   Direnzo, F.; Remoue, F.; Massiani, P.; Fajula, F.; Figueras, F., Influence of Diffusional Barriers on the Thermal-Analysis of the Zeolite TON. *Thermochim. Acta* **1988**, *135*, 359-364.

30.   Trzpit, M.; Soulard, M.; Patarin, J., Water Intrusion in Mesoporous Silicalite-1: An Increase of the Stored Energy. *Micropor. Mesopor. Mat.* **2009**, *117*, 627-634.

31.   Nylen, J.; Sato, T.; Soignard, E.; Yarger, J. L.; Stoyanov, E.; Haussermann, U., Thermal Decomposition of Ammonia Borane at High Pressures. *J. Chem. Phys.* **2009**, *131*, 104506.

32.   Nylen, J.; Eriksson, L.; Benson, D.; Haussermann, U., Characterization of a High Pressure, High Temperature Modification of Ammonia Borane (BH_3NH_3). *J. Chem. Phys.* **2013**, *139*, 054507.

33.   Liu, X. Y.; Su, W. H.; Zhao, X. D.; Wang, Y. F., Transformation of MFI to Beta-Quartz and Coesite under High-Pressure and High-Temperature. *J. Chem. Soc. Chem. Comm.* **1993**, 891-892.

34.   Kuzuba, T.; Era, K.; Ishii, T.; Sato, T., Low-Frequency Raman-Active Vibration of Hexagonal Boron-Nitride. *Solid State Commun.* **1978**, *25*, 863-865.

35.   Li, Y. D.; Garnier, V.; Journet, C.; Barjon, J.; Loiseau, A.; Stenger, I.; Plaud, A.; Toury, B.; Steyer, P., Advanced Synthesis of Highly Crystallized Hexagonal Boron Nitride by Coupling Polymer-Derived Ceramics and Spark Plasma Sintering Processes-Influence of the Crystallization Promoter and Sintering Temperature. *Nanotechnology* **2019**, *30*, 035604.

36.   Yu, K.; Kim, J.; Lee, C.; Jang, A. R.; Shin, H. S.; Kim, K. S.; Yu, Y. J.; Choi, E. J., Infrared Study of Large Scale H-BN Film and Graphene/H-BN Heterostructure. *Appl. Phys. Lett.* **2016**, *108*, 241910.

37.   Frueh, S.; Kellett, R.; Mallery, C.; Molter, T.; Willis, W. S.; King'ondu, C.; Suib, S. L., Pyrolytic Decomposition of Ammonia Borane to Boron Nitride. *Inorg. Chem.* **2011**, *50*, 783-792.

38.   Thomas, J.; Weston, N. E.; Oconnor, T. E., Turbostratic Boron Nitride, Thermal Transformation to Ordered-Layer-Lattice Boron Nitride. *J. Am. Chem. Soc.* **1962**, *84*, 4619-4622.

39.   Abdurahman, A.; Shukla, A.; Dolg, M., Ab Initio Many-Body Calculations on Infinite Carbon and Boron-Nitrogen Chains. *Phys. Rev. B* **2002**, *65*, 115106.

40.	Cretu, O.; Komsa, H. P.; Lehtinen, O.; Algara-Siller, G.; Kaiser, U.; Suenaga, K.; Krasheninnikov, A. V., Experimental Observation of Boron Nitride Chains. *ACS Nano* **2014**, *8*, 11950-11957.

41.	Gao, E. L.; Guo, Y. Z.; Wang, Z. Z.; Nielsen, S. O.; Baughman, R. H., The Strongest and Toughest Predicted Materials: Linear Atomic Chains without a Peierls Instability. *Matter-US* **2022**, *5*, 1192-1203.

42.	Alabarse, F. G.; Rouquette, J.; Coasne, B.; Haidoux, A.; Paulmann, C.; Cambon, O.; Haines, J., Mechanism of H_2O Insertion and Chemical Bond Formation in $AlPO_4$-54·XH_2O at High Pressure. *J. Am. Chem. Soc.* **2015**, *137*, 584-587.

43.	Perdew, J. P., Density Functional Theory and the Band-Gap Problem. *Int. J. Quantum Chem.* **1985**, 497-523.

TOC GRAPHICS
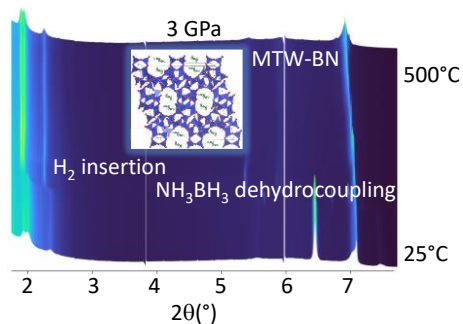
Low dimensional boron nitride (BN) chains were prepared in the one-dimensional pores of the siliceous zeolites TON and MTW by the infiltration followed by the dehydrocoupling and pyrolysis of ammonia borane under high pressure, high temperature conditions. The crystal structures contain one and two one-dimensional zig-zag $(BN)_x$ chains per pore in BN/TON and BN/MTW, respectively. These 1-D BN chains potentially have interesting photoluminescence properties in the far ultraviolet region of the electromagnetic spectrum.